Naval Research Laboratory

Washington, DC 20375-5320

NRL/MR/6750--20-10,187

Considerations in Comparing Experimental Results and Theory of Biased Impedance Probes

David D. Blackwell
Richard F. Fernsler *RETIRED*
William E. Amatucci

Space Physics Simulation Chamber Branch
Plasma Physics Division

David N. Walker

MacAulay-Brown Inc.
Vienna, VA

November 5, 2020

REPORT DOCUMENTATION PAGE

Form Approved
OMB No. 0704-0188

1. REPORT DATE *(DD-MM-YYYY)*	**2. REPORT TYPE**	**3. DATES COVERED** *(From - To)*
05-11-2020	NRL Memorandum Report	06/01/2019 – 08/03/2020

4. TITLE AND SUBTITLE

Considerations in Comparing Experimental Results and Theory of Biased Impedance Probes

5a. CONTRACT NUMBER

5b. GRANT NUMBER

5c. PROGRAM ELEMENT NUMBER

6. AUTHOR(S)

David D. Blackwell, David N. Walker*, Richard F. Fernsler**, and William E. Amatucci

5d. PROJECT NUMBER

5e. TASK NUMBER

5f. WORK UNIT NUMBER
1L46

7. PERFORMING ORGANIZATION NAME(S) AND ADDRESS(ES)

Naval Research Laboratory
4555 Overlook Avenue, SW
Washington, DC 20375-5320

8. PERFORMING ORGANIZATION REPORT NUMBER

NRL/MR/6750--20-10,187

9. SPONSORING / MONITORING AGENCY NAME(S) AND ADDRESS(ES)

Office of Naval Research
One Liberty Center
875 North Randolph Street
Arlington VA 22203-1995

10. SPONSOR / MONITOR'S ACRONYM(S)

11. SPONSOR / MONITOR'S REPORT NUMBER(S)

12. DISTRIBUTION / AVAILABILITY STATEMENT

DISTRIBUTION STATEMENT A: Approved for public release; distribution is unlimited.

13. SUPPLEMENTARY NOTES

* MacAulay-Brown, Inc., 1945 Old Gallows Road, Suite 215, Vienna, VA 22182
**Retired

14. ABSTRACT

This note discuses two outstanding problems that have been present for a number of years in the Space Physics Simulation Chamber group's work on impedance probes. These are, (a) impedance curves indicative of a much higher energy absorption than can be accounted for using standard collision models given the plasma parameters, and (b) divergence at low frequency between predicted and measured impedance curves using our linear model. We compare numerical results of our different models to experimental data to determine under what conditions such models are valid and what areas are in need of improvement.

15. SUBJECT TERMS

Plasma physics Impedance probe Langmuir probe Plasma sheath
Plasma impedance Radiofrequency plasma Plasma diagnostics

16. SECURITY CLASSIFICATION OF:			**17. LIMITATION OF ABSTRACT**	**18. NUMBER OF PAGES**	**19a. NAME OF RESPONSIBLE PERSON**
a. REPORT	**b. ABSTRACT**	**c. THIS PAGE**			David D. Blackwell
Unclassified Unlimited	Unclassified Unlimited	Unclassified Unlimited	Unclassified Unlimited	25	**19b. TELEPHONE NUMBER** *(include area code)* (571) 594-0735

Standard Form 298 (Rev. 8-98)
Prescribed by ANSI Std. Z39.18

This page intentionally left blank.

Considerations in Comparing Experimental Results and Theory of Biased Impedance Probes

David D. Blackwell, David N. Walker*, Richard F. Fernsler†, and William E. Amatucci

U.S. Naval Research Laboratory, Plasma Physics Division Washington, DC

This note discuses two outstanding problems that have been present for a number of years in the Space Physics Simulation Chamber group's work on impedance probes. These are, (a) impedance curves indicative of a much higher energy absorption than can be accounted for using standard collision models given the plasma parameters, and (b) divergence at low frequency between predicted and measured impedance curves using our linear model. We compare numerical results of our different models to experimental data to determine under what conditions such models are valid and what areas are in need of improvement. It is our hope that defining and presenting these problems in a systematic method will help focus future theoretical and experimental efforts in impedance probe research.

I. INTRODUCTION

The plasma impedance probe is a radiofrequency diagnostic that allows the user to infer various plasma properties by observing how the plasma distorts the voltage and current signals of an immersed conducting surface. The voltage and current are applied either between two probes or between a probe and ground. The impedance is calculated either from direct measurements of the voltage and current, or from transmission line reflected power measurements. The probe is remotely located from the measuring equipment, which means the impedance at the measurement point is actually the transmission line transformed impedance at the probe; calibrating the probe to correct for this is the most critical part of the impedance measurement.

As mentioned, two problems in our impedance probe work have been centered on the divergence between measured results and theoretically predicted results. The first of these

* MacAulay-Brown Inc

† NRL Plasma Physics Div.,(ret)

Manuscript approved October 16, 2020.

problems, large energy absorption that could not be explained with collisions, was mentioned in the very first impedance probe papers published by our group [3][4], and subsequently led to theoretical models of collisionless impedance [8]. The second of these problems arose from our experiments to determine secondary plasma data such as electron temperature and plasma potential[9][5] from impedance variations vs bias voltage.

These divergences of experiment and theory are rooted in the same problem. That is, these diagnostics are very capable of measuring plasma parameters that can be obtained from clear transitions visible in the characteristics; they are also very capable of measuring relative changes in plasma parameters. They are less reliable, however, measuring absolute numbers. For example, the electron density is derived from the upper hybrid frequency, is a resonance of the impedance where $\mathbb{I}\mathrm{m}\{Z\} = 0$, so it is robustly identifiable; the plasma potential appears as a minimum in the real part of the impedance and tracks with another resonance. There are clear inflection points that can be pointed to on a graph. For other parts of the models of the impedance probe, are there such inflection points that can definitively tell us that the models are correct? How are the models experimentally falsifiable? These are the questions we're trying to answer in this note. It is our aim that the results here will better define areas of uncertainty and possible experimental improvement.

II. LINEAR MODEL

It is instructive at this point to use as the starting point a derivation of the linear model to which experimental comparisons are made. A simple beginning is to write the total impedance between the probe surface and ground through the plasma as a series combination of the sheath and bulk plasma impedance:

$$Z = Z_{sh} + Z_p \tag{1}$$

with Z_{sh} and Z_p the respective sheath and plasma impedances. The plasma impedance can be derived by first assuming a uniform sphere (chosen for simplicity, but this could apply to other geometries) immersed in a plasma for which we can write

$$\oint_S \vec{E}\,(r) \bullet d\vec{s} = \frac{Q}{\epsilon_0} + \frac{1}{\epsilon_0}\int_V \rho dV \tag{2}$$

where Q is the surface charge of the sphere. Combining this with the continuity equation

assuming an $e^{i\omega t}$ time dependence as

$$\nabla \bullet \vec{J} = -i\omega\rho \tag{3}$$

lets us rewrite 2 as

$$\begin{aligned} E(r)\,4\pi r^2 &= \frac{Q}{\epsilon_0} + \frac{1}{\epsilon_0}\int_V \frac{\nabla \bullet \vec{J}}{-i\omega} dV \\ &= \frac{Q}{\epsilon_0} + \frac{1}{\epsilon_0}\oint_S \frac{\vec{J} \bullet d\vec{s}}{-i\omega} \\ &= \frac{Q}{\epsilon_0} + \frac{1}{\epsilon_0}\frac{J(r)\,4\pi r^2}{-i\omega} \end{aligned} \tag{4}$$

The current $J(r) = -en_0 v$ can be found from the electron equation of motion

$$i\omega m n_0 v = -en_0 E - mn_0 \nu v \tag{5}$$

with n_0 the electron density, ν the effective collision frequency, and m the electron mass. We can write J as

$$J = \frac{e^2 n_0 E}{im(\omega - i\nu)} \tag{6}$$

Substituting 6 into 4 and combining like terms gives

$$E(r) = \frac{Q}{\epsilon_0 4\pi r^2}\left(1 - \frac{\omega_p^2}{\omega(\omega - i\nu)}\right)^{-1} \tag{7}$$

Given an expression for $E(r)$ we can calculate the voltage integrating the radius from the probe radius ρ to infinity to get

$$V = -\frac{Q}{4\pi\epsilon_0}\int_\rho^\infty \left(1 - \frac{\omega_p^2}{\omega(\omega - i\nu)}\right)^{-1} \frac{dr}{r^2} \tag{8}$$

This is the general expression between the voltage and charge of a sphere with an oscillating potential immersed in a plasma. For the special case of a uniform plasma, we can see that the capacitance is readily defined as

$$C = 4\pi\epsilon_0\left(1 - \frac{\omega_p^2}{\omega(\omega - i\nu)}\right)\rho \tag{9}$$

This is the same expression from the 2005 RSI paper [3]. At this point in that paper we assumed a vacuum sheath, but now we're going to modify that model a bit.

III. INTEGRATING THROUGH THE SHEATH AND COLLISONLESS RESISTANCE

The linearized small signal impedance model for our sphere starts with the expression for impedance derived from Maxwell's equations and the electron equation of motion found in the 2006 Phys. Plasmas article[8], which is just a rewriting of 8:

$$Z = \frac{1}{4\pi\epsilon_0}\int_{\rho}^{\infty} \frac{\nu + i\omega}{\omega_p^2(r) - \omega^2 + i\omega\nu}\frac{dr}{r^2} \tag{10}$$

The only term in the integrand that is a function of r is the plasma frequency ω_p, and it only varies over the plasma sheath. If the plasma frequency beyond the sheath can be represented as ω_{pe}, then the integral can be broken into two parts as

$$Z = Z_{sh} + \frac{1}{4\pi\epsilon_0(\rho + s)}\frac{\nu + i\omega}{\omega_{pe}^2 - \omega^2 + i\omega\nu} \tag{11}$$

with

$$Z_{sh} = \frac{1}{4\pi\epsilon_0}\int_{\rho}^{s} \frac{\nu + i\omega}{\omega_{pe}^2 - \omega^2 + i\omega\nu}\frac{dr}{r^2} \tag{12}$$

The second term is a rewriting of the expression $Z_p = \dfrac{1}{i\omega C_0' + \dfrac{1}{R_p + i\omega L_p}}$, which is the contribution of the bulk plasma to the impedance with circuit elements written in terms of plasma parameters as

$$\begin{aligned} C_0' &= 4\pi\epsilon_0(\rho + s) \\ L_p &= \omega_{pe}^{-2} C_0'^{-1} \\ R &= \nu L_p \end{aligned}$$

In all expressions s is the sheath width, which is a function of the probe surface voltage. To calculate 12, we must consider the type of sheath profile to use.

A. sheath profiles

1. *Modified Child Langmuir*

This is the model that was used to determine the sheath capacitance in the biased impedance probe paper [4]. The potential function within the sheath using this model

is

$$\Phi(x) = \phi \times \left(\frac{s(\phi) + \rho - x}{s(\phi)} \right)^{\frac{5}{2}} \tag{13}$$

with

$$s(\phi) = \left(2.5 - 1.87e^{-0.39\frac{\rho}{\lambda_d}}\right) \left(\frac{e\phi}{kT_e}\right)^{\frac{2}{5}} \lambda_d$$

Here ϕ is the voltage on the surface of the probe and λ_d the Debye length. This has the advantage that you specify the probe voltage first and it calculates a sheath width; the next two models don't.

2. Sheath as solution to the Poisson equation I

This somewhat follows the method laid out in Chen[14]. The Poisson equation (equation 8-8, page 292 in the book) can be written in spherical coordinates as

$$\frac{1}{r^2}\frac{\partial}{\partial r}\left(r^2 \frac{\partial}{\partial r}\phi\right) = \frac{e}{\epsilon_0} n_e \left(e^{-\frac{\phi}{kT_e}} - \frac{r_s^2}{r^2}\left(1 - \frac{2\phi}{kT_e}\right)^{-1/2} \right) \tag{14}$$

Here n_e is the bulk electron density and r_s is the sheath edge. Specifying the boundary conditions at the sheath edge that $\phi(r_s)$ and $\phi(r_s)$ are both zero allows the Poisson equation to be solved numerically. In this case r_s is specified and we solve for the probe voltage.

3. Sheath as solution to the Poisson equation II

In the 2009 paper by Fernsler [15] the Poisson equation is again solved numerically. This time the equation is written as

$$\frac{1}{\chi^2}\frac{d}{d\chi}\chi^2 \frac{d\Phi}{d\chi} = \left(\frac{\chi_0}{\chi}\right)^2 \frac{\gamma}{\sqrt{\Phi}} - e^{\Phi} \tag{15}$$

with $\chi = r/\lambda_D$, $\Phi = -e\phi/T_e$, $\chi_0 = r_0/\lambda_D$, and λ_D is the electron Debye length. The solution is slightly different in that the boundary conditions are that the right side of equation 15 and its first derivative are both set to zero at a position outside the sheath. Starting at this position the sheath and presheath are solved for iteratively going inward.

4. Comparison of the different solutions

Figure 1 shows voltage and normalized electron density vs. number of Debye lengths from the probe surface for a typical plasma with $n_e = 1.25 \times 10^8$ cm^{-3}, $T_e = 2.4$ eV, and an

electron-neutral collision frequency of 3.57×10^6 Hz. In this particular plot I chose a starting point for Fernsler's numerical method of 50 Debye lengths from the probe, using that result calculated the Child-Langmuir sheath, and adjusted the sheath width in Chen's model to get the same probe voltage. The modified Child-Langmuir sheath gave an almost identical result as the numerical integration of equation 14, while the numerical solution outlined in the 2009 paper gives a more gradual potential and thicker sheath.

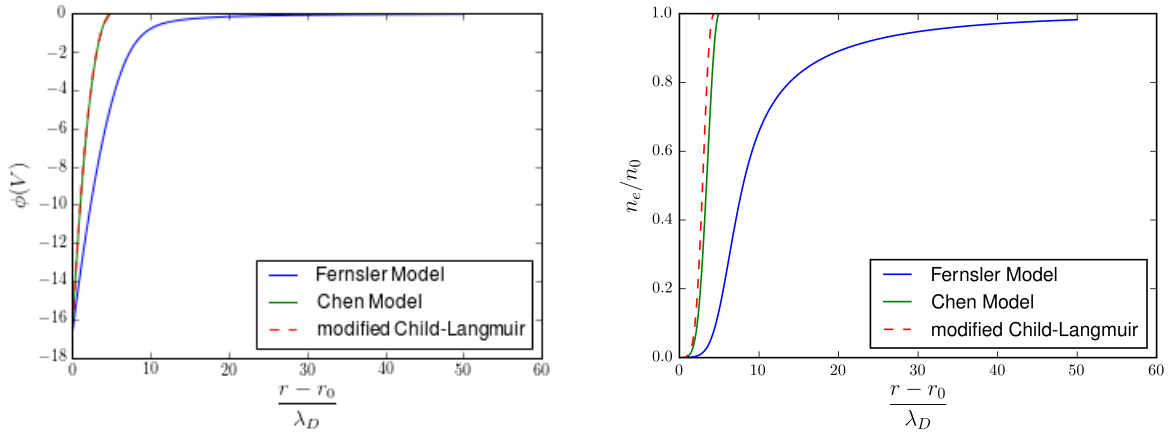

(a)Sheath voltage

(b)Sheath density

FIG. 1: Sheath voltage relative to plasma potential and normalized electron density for a plasma with $n_e = 1.25 \times 10^8$ cm^{-3}, $T_e = 2.4$ eV, $\nu = 3.57 \times 10^6$ Hz for a 3-inch diameter spherical probe

B. Integrated Impedance

Once we have the electron density profile we can perform the integration of equation 11; there are different ways of doing this. First, following the reasonable assumption of a collisionless sheath, we set $\nu \to 0$ to arrive at an expression for Z_{sh} of

$$Z_{sh} = \frac{1}{4\pi\epsilon_0} \int_\rho^s \frac{i\omega}{\omega_{pe}^2 - \omega^2} \frac{dr}{r^2} \tag{16}$$

which is in fact equation 9 in the 2006 Phys. Plasmas paper. Depending on the value of ω, it is possible for there to be a pole in the integrand, in which case the integral must be done as a contour integral in the upper half of the complex plane. The result of such an

integration is expressed in equation 10 from the same paper as

$$Z_{sh} = \frac{i\omega P}{4\pi\epsilon_0} + \frac{\omega}{4\pi\epsilon_0 r_r^2}\left[\frac{d\omega_{pe}}{dr}\right]^{-1} \tag{17}$$

Where here r_r is the radius at which $\omega = \omega_{pe}$. Although not explicitly written in the paper, the principle value P is the integral excluding the the singularity, which can be written as

$$P = \lim_{\delta\to 0}\left(\int_{\rho}^{r_r-\delta} I dr + \int_{r_r+\delta}^{s} I dr\right) \tag{18}$$

where I is the integrand of equation 16. Equation 18 can be calculated numerically by taking a large number of radial points($\approx$ 5000) and reducing δ until a stable answer is reached. Another method of evaluating Z_{sh} is to leave the collision frequency in place and simply perform the integral numerically. In this case there is no need for contour integration or residues. Whichever method we use, the size of Z_{sh} will vary greatly depending on whether we integrate through the point where the RF frequency is equal to the local plasma frequency. The location of this point, or resonant radius, will be a function of both voltage and applied frequency. Figure 2 shows how this location changes for a fixed frequency, with smaller probe biases moving the resonant radius closer to the probe. For simplicity I used the Child-Langmuir sheath in this calculation, but small changes in the sheath structure from the other methods do not alter the results significantly.

We can see that depending on what frequency we choose, sometimes we will integrate through the resonance, and sometimes we won't. This has a dramatic effect on the impedance curve; figure 3 shows the real and imaginary parts of the impedance vs ω using both sheath profiles and both methods of integration. Since the Chen and Child-Langmuir sheaths are practically identical only one of these is computed (the Child-Langmuir, since it is faster to compute) and compared with results with the Fernsler model. For now the probe voltage is -10 V relative to the plasma potential as it is in figure 1. Figure 4 shows the real part of the impedance vs voltage under the same conditions with the frequency fixed at $\omega = \omega_{pe}/10$. The presence of the resonance in the integrand of 12 creates a dividing line in frequency and voltage space that is easy to pick out in the 2-D plots of figure 5. In these plots I have used a plasma density of $n_e = 4\times 10^7 \mathrm{cm}^{-3}$, a probe radius of 1.5 in., and an electron temperature of 2.4 eV; these numbers are identical to 2-D experimental data at these conditions taken in March 2013. For comparison a plot constructed from experimental measurements under

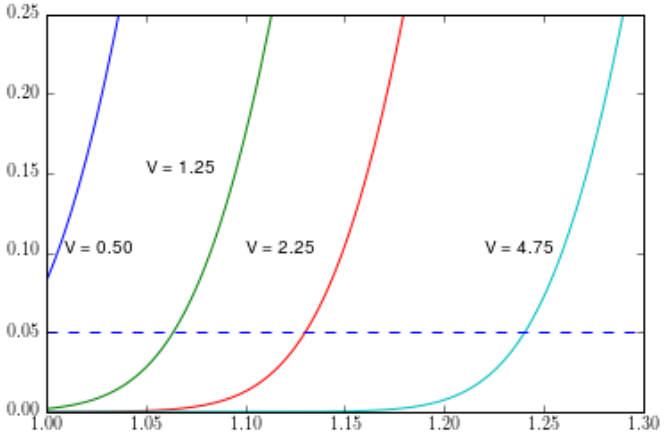

FIG. 2: The intersection of applied frequency $\omega/\omega_p = 0.05$ and local plasma frequency curve as the probe voltage is changed for a plasma with $n_e = 4.15 \times 10^7 \text{cm}^{-3}$, $T_e = 0.1\text{eV}$, and a spherical probe with radius $r_0 = 1\text{cm}$. As the probe voltage is decreased, the resonant radius moves closer to the probe, and at small enough voltage and low enough frequency, there is no resonant radius.

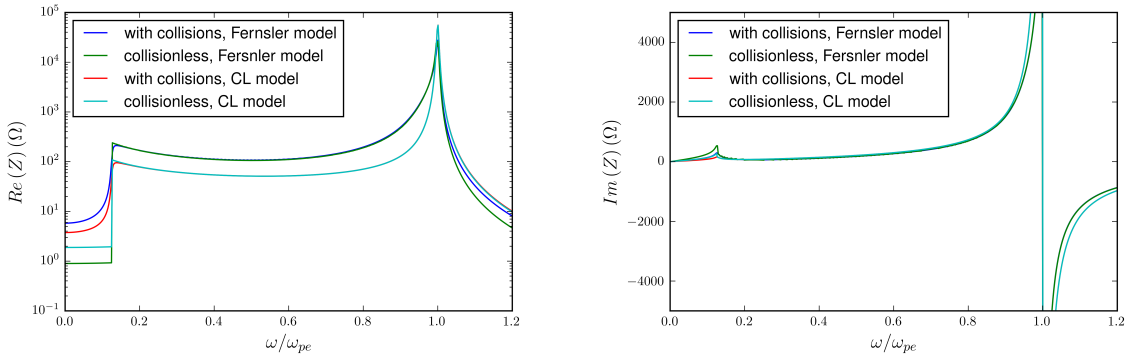

FIG. 3: The real and imaginary parts of the impedance for the conditions used in the sheath calculations of Figure 1.

the same conditions is also shown in figure 6

IV. AD HOC SHEATH MODEL

We again begin with our expression for impedance from equation 1 where we write

$$Z = Z_{sh} + Z_p \tag{19}$$

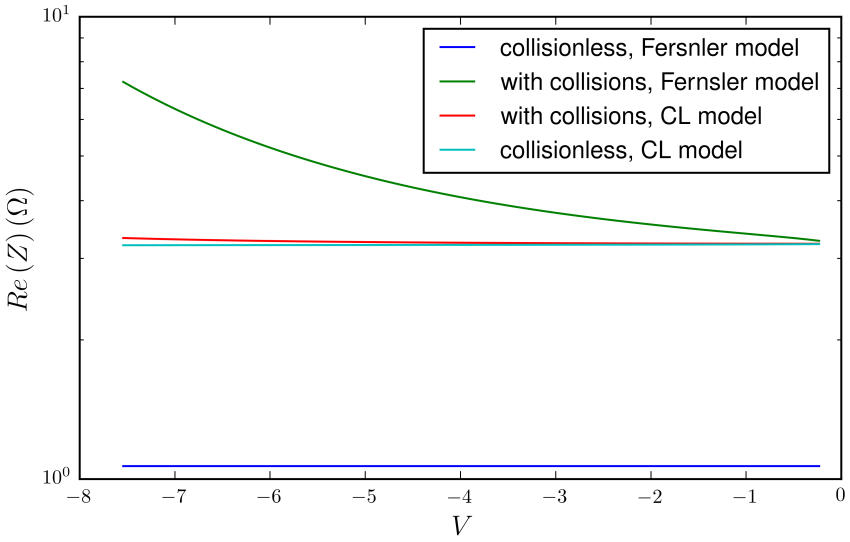

FIG. 4: The real part of the impedance vs voltage with $\omega = \omega_{pe}/10$ under the same conditions as the previous plots.

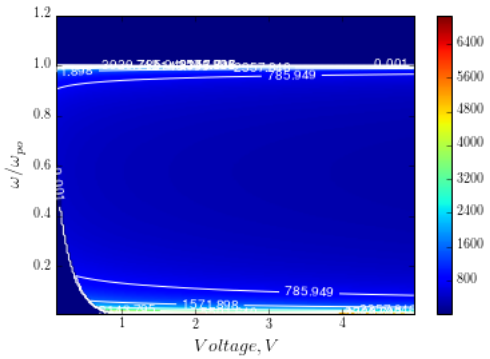

(a)Collisionless resistance vs frequency and probe voltage; the dark blue region on the left side of the curve marks the dividing line where the resistance vanishes

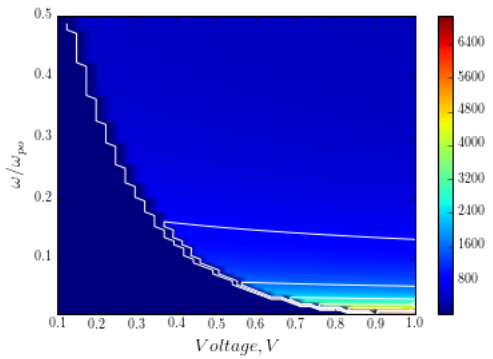

(b)An expanded axis view of 5(a) to better show the contours of R at low frequency

FIG. 5: A 2-D plot of collisionless resistance vs probe voltage and frequency.

but now we will calculate the Z_{sh} term in a different way. The sheath thickness is a function of the potential difference between the probe and the plasma, so that when that potential oscillates, the sheath thickness will oscillate as well. The electrons reflected from the sheath edge are then effectively in motion with respect to the probe, and the displacement current

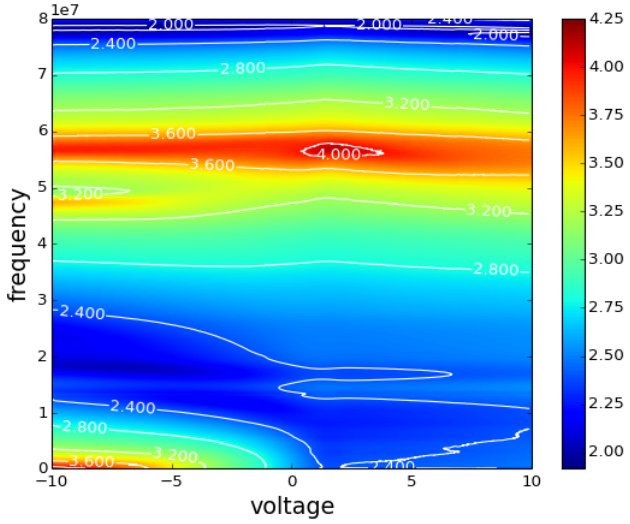

FIG. 6: The magnitude of the impedance, Z, measured with the same probe and plasma conditions as the calculated curves of Figure 5.

due to their motion can be written as

$$i_e = eA_{sh}n_0v_{sh} \tag{20}$$

where A_{sh} is the area of the sheath and v_{sh} is the velocity of the sheath edge. Now this velocity can be written as $\frac{ds}{dt}$ with $s = s(V)$ the sheath thickness as a function of V, the potential difference between the probe and the plasma. We can rewrite the displacement current from 20 as

$$i_e = eA_{sh}n_0\frac{\partial s}{\partial V}\frac{dV}{dt}$$

$$= i\omega C_{sh}V \tag{21}$$

where now we have defined the sheath capacitance as

$$C_{sh}(V) = eA_{sh}n_0\frac{\partial s}{\partial V} \tag{22}$$

The total current to the probe can be written as the sum of the conduction and displacement currents as

$$i_p = i_c(V) + i\omega C_{sh}V \tag{23}$$

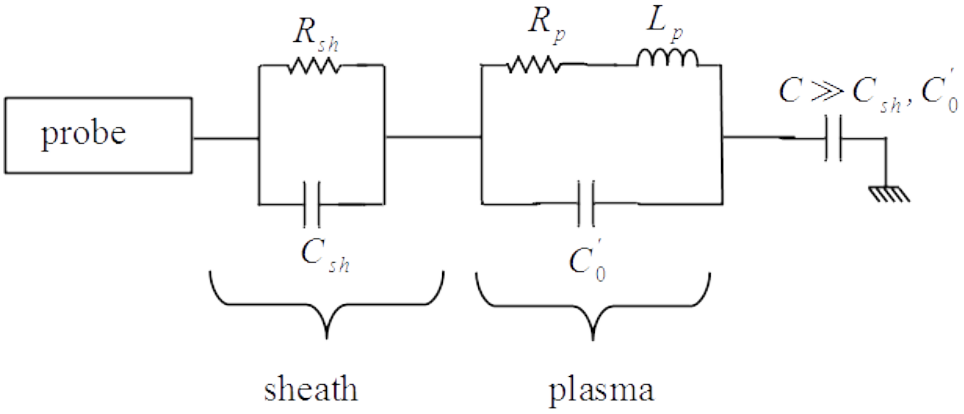

FIG. 7: Circuit model of the plasma-probe impedance using equation 25.

which, if we allow that we can write $i_c(V) = V/R_{sh}$, with R_{sh} the sheath resistance, becomes

$$i_p = \frac{V}{R_{sh}} + i\omega C_{sh} V \tag{24}$$

Note the assumption being made here: the sheath resistance R_{sh} is derived from the steady state equations of motion, so this requires the electrons pass through the sheath much faster than the period of the oscillating voltage. If the time for an electron to travel one Debye length is much less than one RF period, the sheath transit time can be said to be small.

The impedance of the plasma and probe together can now be modeled using the circuit shown in figure 7, such that

$$Z = \frac{1}{\frac{1}{R_{sh}} + i\omega C_{sh}} + \frac{1}{i\omega C_0' + \frac{1}{R_p + i\omega L_p}} \tag{25}$$

with circuit elements written in terms of the plasma parameters as

$$\begin{aligned} C_0' &= 4\pi\epsilon_0(\rho + s) \\ L_p &= \omega_{pe}^{-2} C_0'^{-1} \\ R &= \nu L_p \end{aligned}$$

where s is the sheath width. The second part of this equation is the integral of equation 8 integrated out from the edge of the sheath. This is almost the same as equation (1) in the 2005 RSI paper except now a sheath resistance is in parallel with the sheath capacitance, and the vacuum capacitance of the sphere is larger by a factor of $\frac{\rho + s}{\rho}$. It is physically more realistic as the expression reduces to just the DC resistance, R_{sh}, at low frequencies.

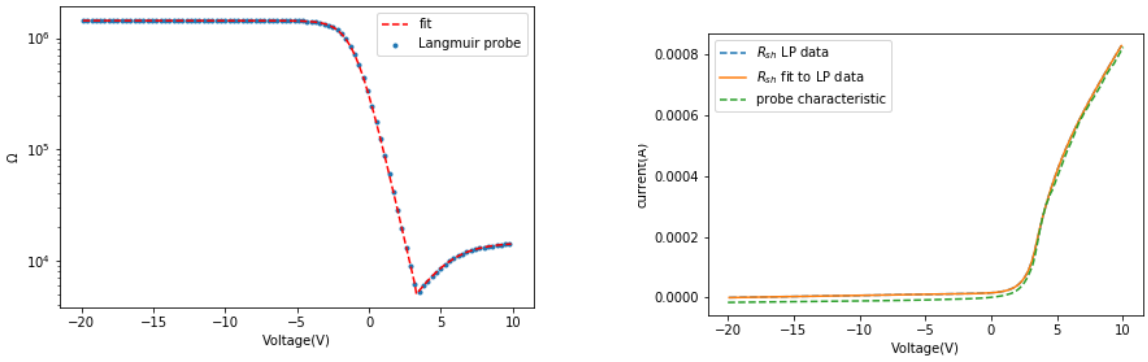

(a) (b)

FIG. 8: (a) R_{sh} from Langmuir probe data with curve fit for a 1" diameter probe and a plasma density of $8.4 \times 10^6 \text{cm}^{-3}$ with $T_e = 0.75\text{eV}$. (b) The original Langmuir probe characteristic along with the reconstructed curves from R_{sh} and the curve fit.

The sheath resistance R_{sh}, capacitance C_{sh}, and sheath thickness s in equations 25 are functions of the probe DC voltage V_0. I'm going to use the same sheath thickness from equation 13. With this sheath thickness and equation 22, we can write

$$C_{sh} = 0.4en_0A\frac{s\left(\phi\right)}{\phi} \tag{26}$$

The R_{sh} term can be constructed from experimental curves using the impedance probe as a Langmuir probe, with R_{sh} defined as

$$\frac{1}{R_{sh}} \equiv \frac{\partial i_c(V)}{\partial V} \tag{27}$$

which is consistent with its use in equation 24. Two curve fits of the form $R_{sh}\left(V\right) = a_0 + a_1 arctanh\left[\left(V + a_2\right)/a_3\right]$ could be fit to the experimental value of R_{sh}. Figure 8 shows the experimental sheath resistance, the curve fit, and the reciprocals of the integrated curve fit and integrated sheath resistance compared to the original Langmuir probe curve.

When the probe is positively biased, the electron sheath impedance was previously calculated using Llwellyn-Peterson coefficients [11][12] in the second 2005 paper [4], which gives a rather lengthy expression for the electron sheath impedance as

$$Z^+\left(\beta, T\right) = \frac{T^2}{2\beta}\left[1 - \frac{\zeta}{3}\left(1 - \frac{12S\left(\beta\right)}{\beta^3}\right)\right]\frac{\left(v_{th} + v_e\right)}{4\pi\varepsilon_0\rho^2} \tag{28}$$

with

$$\beta = i\omega T \qquad v_{th} = \sqrt{\frac{kT_e}{m}}$$
$$v_e = \sqrt{\frac{2e\phi}{m}} \qquad \zeta = \frac{v_{th} - v_e}{v_{th} + v_e}$$
$$S(\beta) = 2 - 2e^{-\beta} - \beta - \beta e^{-\beta} \tag{29}$$

Here the sheath transit time is given by

$$T = \int_0^{s(\phi)} v_{th}^{-1} \left(1 + \frac{e\Phi(x)}{kT_e}\right)^{-\frac{1}{2}} \tag{30}$$

with the potential function $\Phi(x)$ and sheath thickness $s(\phi)$ referring now to the electron sheath; for simplicity we used the same Child-Langmuir type expression as in equation 13.

Now we're going to make two changes to this expression. The first change is that equation 28 can be tremendously simplified for frequencies below the plasma frequency into a simple expression of sheath capacitance as a function of voltage

$$Z^+(\omega, v) = \frac{1}{j\omega C_{sh}^e(v)} \tag{31}$$

with

$$C_{sh}^e(v) = \frac{\epsilon_0 A}{v_{th} T(v)}$$

The second change will be including the DC sheath resistance term in the impedance the same way we did for the ion sheath, using the curve fit to R_{sh} from the Langmuir probe data. This sheath impedance will be in series with the rest of the plasma impedance, i.e., the second term of equation 25. The general expression for impedance then becomes

$$Z = \frac{1}{\frac{1}{R_{sh}} + i\omega C_{sh}} + \frac{1}{i\omega C_0' + \frac{1}{R_p + i\omega L_p}} \tag{32}$$

with

$$C_{sh} = 0.4 e n_0 A \frac{s(\phi)}{\phi} \qquad \phi < 0$$
$$C_{sh}(v) = \frac{\epsilon_0 A}{v_{th} T(\phi)} \qquad \phi > 0$$

where C_0', R_P and L_P are all evaluated at $s = 0$ for the electron sheath. This impedance is similar to that used in the 2008 Phys. Plasmas paper [9], which had the expression for the sheath impedance as

$$Z_{sh} = \frac{1}{i\omega C_{sh} + \dfrac{1}{R_{sh} + i\omega L_{sh}}} \tag{33}$$

with L_{sh} the sheath inductance, which is small enough to be neglected [9] in conditions of our experiments. This ad-hoc model of impedance differs only in the sheath impedance term from the integrated model; the bulk plasma terms are the same for both. This model relies on the assumption that the sheath resistance R_{sh} is the same as the DC resistance even though we are applying an AC signal to the probe, so the requirement is that the amplitude of the AC voltage is small enough to be neglected in considering electron motion through the sheath. In other words the AC sheath impedance is a small signal perturbation around a DC operating point.

V. DISCUSSION

A. Problems with the integrated sheath model

The integrated sheath model, again, consists of integrating the dielectric constant of the plasma, ϵ_p, from the surface of the probe out to the some very large distance from the probe, usually several probe radii. This means integrating equation 10 from the probe surface outwards. Whether by integrating in the complex plane or by including a finite collision frequency, in all cases this gives the unrealistic result of a discontinuity. The discontinuity that is introduced comes not from the shape of the density gradient in the sheath, but from the fact that in the sheath, for certain frequencies, the expression for impedance given in [8]

$$Z = \frac{1}{4\pi\epsilon_0}\int_{r_0}^{\infty}\frac{dr}{r^2}\frac{\nu + i\omega}{\left(\omega_p^2 - \omega^2\right) + i\omega\nu} \tag{34}$$

will contain a pole in the integrand, namely where $\omega_{p0} < \omega < \omega_p$, with ω_{p0} the value of the plasma frequency at the probe surface. If the applied frequency ω is outside of the range, there is no pole and thus no collisionless resistance (which is plainly stated in [8]). This discontinuity is thus a feature of this formulation, and won't be smoothed over by choosing different sheath profiles. This discontinuity is not observed in the experimental

data. Figures 10-12 are 2-D plots of $\mathbb{R}\mathrm{e}\{Z\}$ and $-\mathbb{I}\mathrm{m}\{Z\}$ from experimental data, from the integrated impedance model, and from the ad-hoc impedance model. For maximum utility of comparison, both quantities are shown on a logarithmic scale, as is the frequency axis normalized to ω_p. The second row of plots is the integrated impedance model; the discontinuity in the real part of impedance over a wide frequency range is quite clearly visible. Another serious problem with this model is that all of the real part of the sheath impedance, for a collisionless sheath, comes from this collisionless resistance. There is no provision for including the DC sheath resistance R_{sh}, and thus no possibility of the model converging to that value at low frequency.

B. problems with the ad-hoc model

The ad-hoc model makes physical sense; at low frequencies ($\omega \longrightarrow 0$) it goes to the DC value R_{sh}. The function for R_{sh} used in the model is a fit to the sheath resistance derived from the experimental Langmuir probe characteristic. With this model, it can also be shown at low frequencies that the real part of 32, dominated by the sheath impedance, can be written as [9]

$$\mathbb{R}\mathrm{e}\{Z\} = \frac{R_{sh}}{1 + (\omega C_{sh} Rsh)^2} \tag{35}$$

This curve has an inflection point at $R_{sh} = \dfrac{1}{\omega C_{sh}}$. This is in agreement with the measured data, which also has an inflection point in $\mathbb{R}\mathrm{e}\{Z\}$, which can be seen in comparisons between the two in figures 10 to 12. A more quantitative comparison can be found in the same paper[9] by solving for the sheath resistance as

$$R_{sh} = \mathbb{R}\mathrm{e}\{Z\} \left(1 + \left[\frac{\mathbb{I}\mathrm{m}\{Z\}}{\mathbb{R}\mathrm{e}\{Z\}}\right]^2\right) \tag{36}$$

We can compare this sheath resistance to that derived from the Langmuir probe characteristic as a check; we can also integrate the reciprocal of this sheath resistance and compare that to the probe characteristic. When this was done we start to get large differences in the curves for R_{sh}, as seen in figure 9. The curves still have the same shape, but the Langmuir probe value of R_{sh} is always much larger than that derived from the impedance probe. This problem gets worse with lower plasma density. This could be because the very nature of the measurement can lead to inaccuracies at low frequencies. We are obtaining the real part of

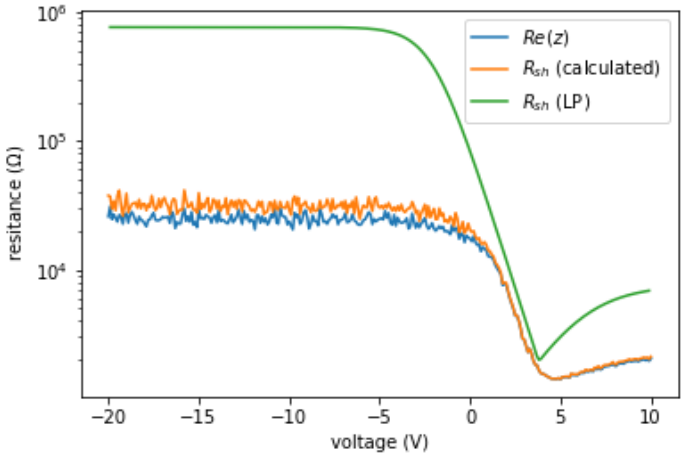

FIG. 9: R_{sh} calculated from the impedance probe using equation 36, $\mathbb{R}\mathrm{e}\{Z\}$, and R_{sh} from the Langmuir probe characteristic for a 1" diameter spherical impedance probe in a plasma with a plasma density of $n_e = 1.9 \times 10^7 \mathrm{cm}^{-3}$ and $T_e = 1.0\mathrm{eV}$

Z from the reflection coefficient Γ through the relation $\Gamma = \dfrac{Z-50}{Z+50}$, and this measurement becomes very insensitive to changes in $\mathbb{R}\mathrm{e}\{Z\}$ if $\mathbb{R}\mathrm{e}\{Z\}$ is very large compared to 50Ω and $\mathbb{I}\mathrm{m}\{Z\}$ is very small. If we look at the curves for R_{sh} from Langmuir probe data all plotted together, and compare that with R_{sh} curves from the impedance probe, we observe that the impedance probe curves have less vertical resolution as the density decreases, and that the curves all tend to have maximum values somewhat close to one another. The Langmuir probe impedance curves on the other hand vary greatly in vertical range even at low density. This could indicate that the Agilent 5061 Network analyzer simply cannot resolve the differences between 10 kΩ and 100 kΩ reliably, so an alternative method of obtaining the measured impedance, along with a more definitive test of the analyzer's capability in this range of impedances and frequencies, would be required to resolve this.

VI. CONCLUSIONS

The issue remaining with an accurate model of the plasma impedance is resolving how to model the impedance of the sheath. In the first rendering [3], the sheath was treated as strictly capacitive. Soon after, this was improved by applying the linearized equations of electron motion to electrons in the sheath region as well, and integrating over the density

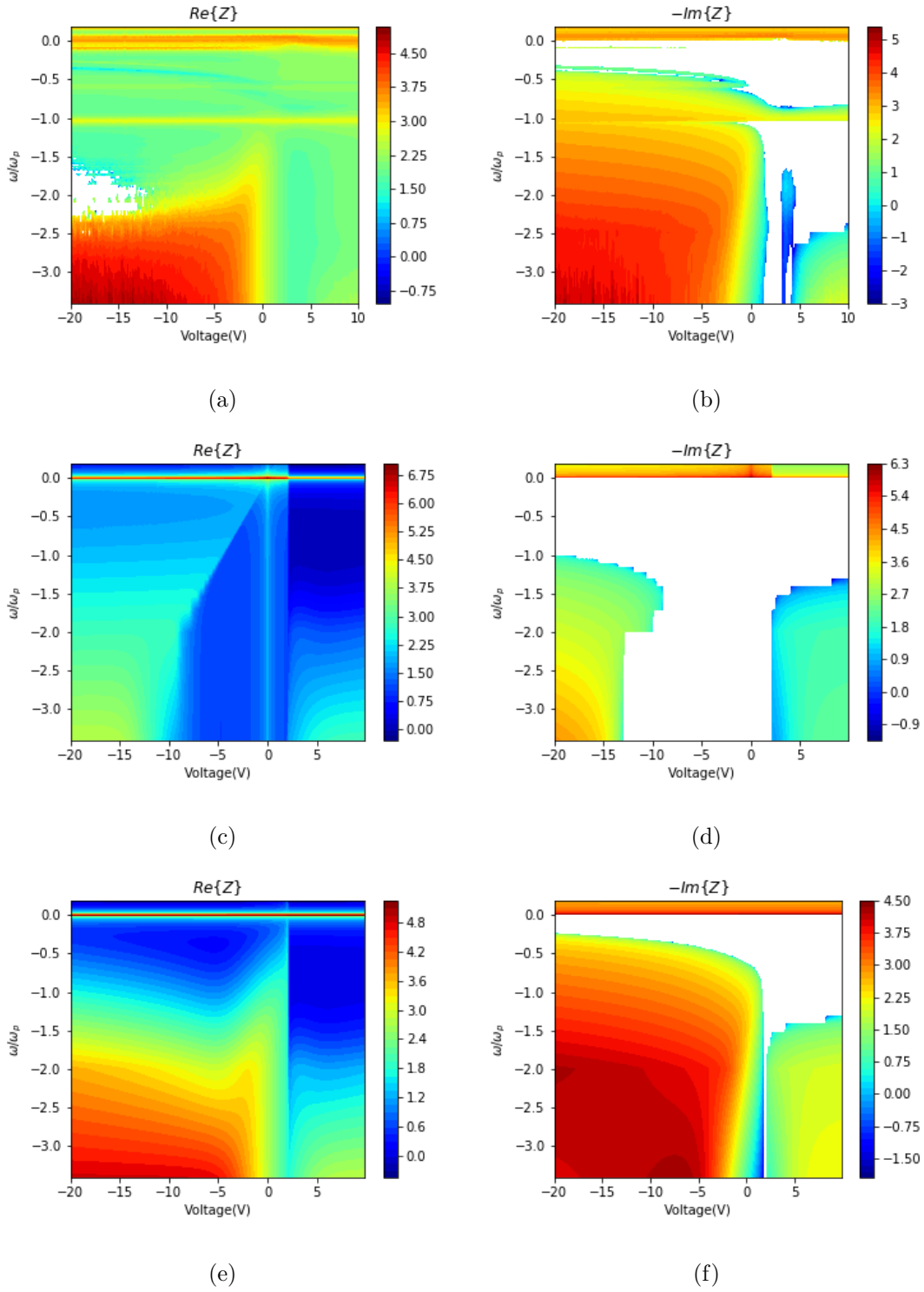

FIG. 10: Filled contour plots of real and imaginary impedance with both amplitude and normalized frequency on logarithmic scales; (a) and (b) represent impedance obtained from reflected power measurements, (c) and (d) are calculated using the integrated impedance model, while (e) and (f) are calculated with the ad-hoc impedance model. The electron density is estimated at $n_e \approx 9 \times 10^8 \mathrm{cm}^{-3}$ with $T_e \approx 1.0\mathrm{eV}$ from Langmuir and impedance probe measurements with a 1.0 inch diameter sphere.

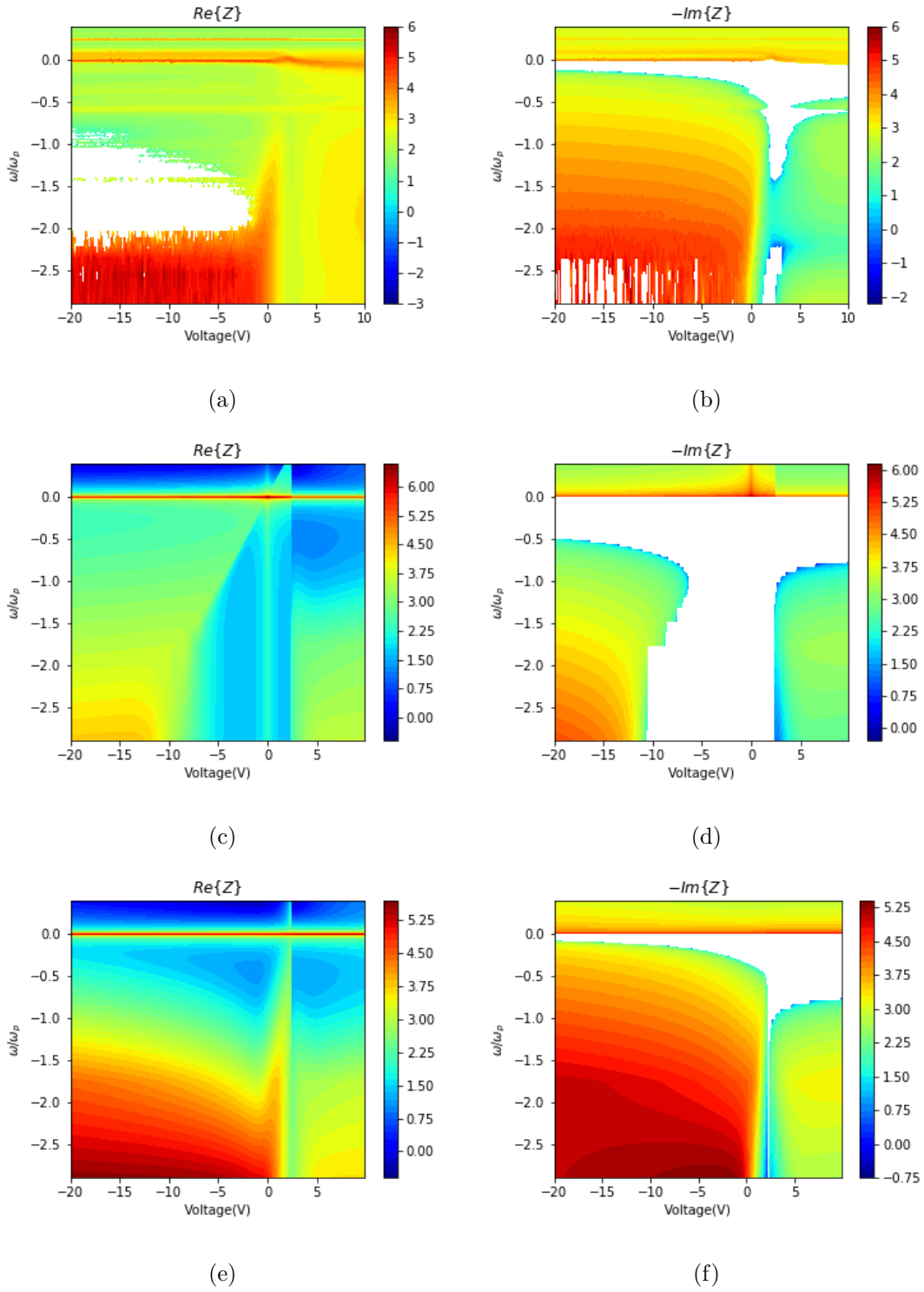

FIG. 11: The same plots from the previous figure 10 with an electron density $n_e \approx 7 \times 10^7 \text{cm}^{-3}$ with $T_e \approx 1.0\text{eV}$ from Langmuir and impedance probe measurements with a 1.0 inch diameter sphere.

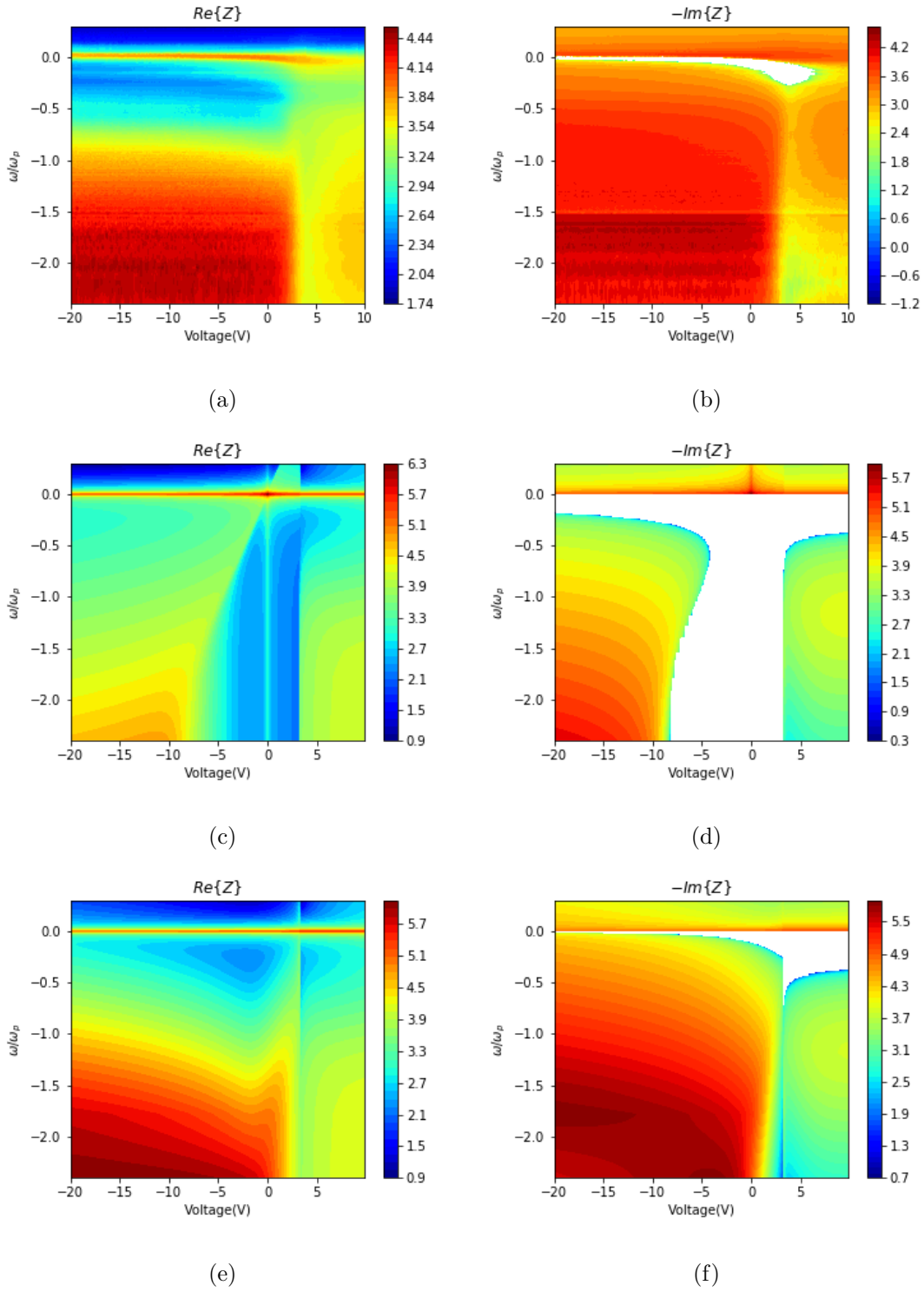

FIG. 12: The same plots from the previous figure 10 with an electron density $n_e \approx 8 \times 10^6 \text{cm}^{-3}$ with $T_e \approx 1.0\text{eV}$ from Langmuir and impedance probe measurements with a 1.0 inch diameter sphere.

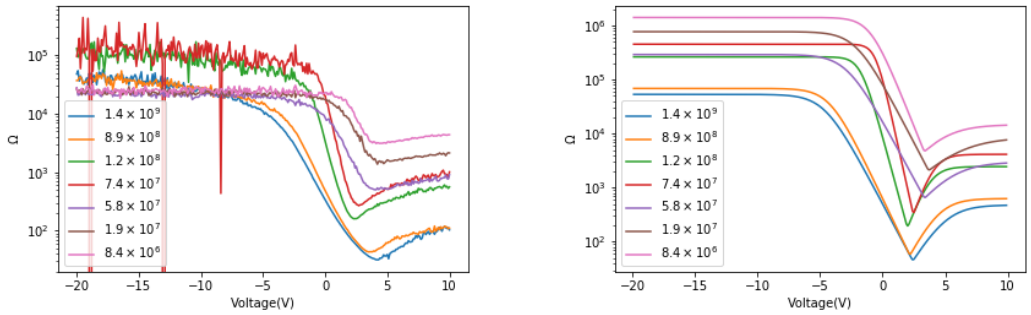

(a) (b)

FIG. 13: Plots of $\mathbb{R}\mathrm{e}\{Z\}$ from the impedance probe at low frequency ($f < 100kHz$) and R_{sh} from Langmuir probe traces for various electron densities (in cm^{-3}).

gradient in the sheath. Whether by integrating in the complex plane or by including a finite collision frequency, in all cases this gives the unrealistic result of a discontinuity. The third model attempted, in which expressions for sheath resistance and capacitance are used in a more heuristic approach, reproduces many of the features of the actual data. However this also diverges from measurements at low frequencies, where it predicts a numerically smaller $\mathbb{R}\mathrm{e}\{Z\} \approx R_{sh}$. Even so, the ad-hoc model gives the best predictions to date of the experimental measurements, and the observed discrepancy in the real part could possibly be corrected using a more accurate method of obtaining large values of Z at low frequency.

VII. APPENDIX: LIMITATIONS OF THE REFLECTED POWER IMPEDANCE MEASUREMENT

It is important to be aware of the limitations of measuring the impedance using the network analyzer's reflected power measurement. We are not measuring impedance directly, but calculating impedance from the magnitude and phase of the reflected power. The two are related through the relation

$$Z = Z_0 \times \frac{1+\Gamma}{1-\Gamma} \tag{37}$$

where Γ is the complex reflection coefficient, which is S-parameter S_{11} from the network analyzer. The actual network analyzer has an uncertainty in both magnitude and phase of Γ, such that we can rewrite

$$\Gamma \longrightarrow (|\Gamma| + |\delta\Gamma|)\, e^{\phi+\delta\phi} \tag{38}$$

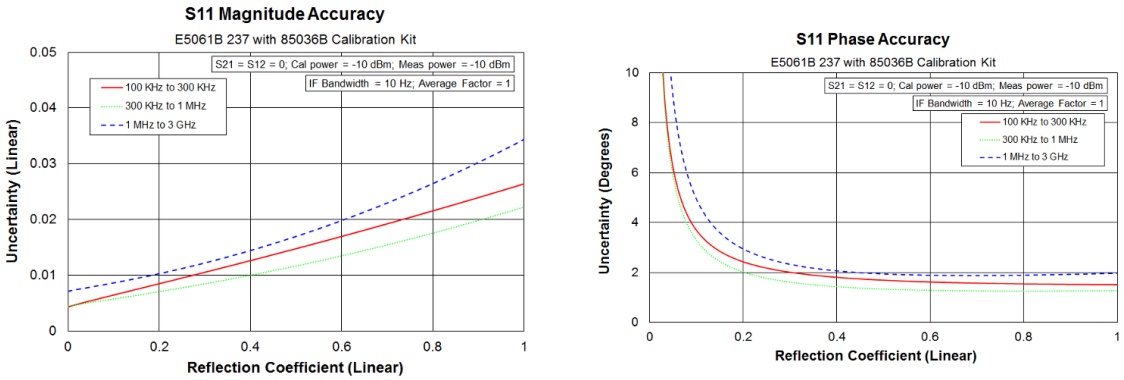

FIG. 14: Uncertainty in reflection coefficient S_{11}; from the Agilent E5061A user manual

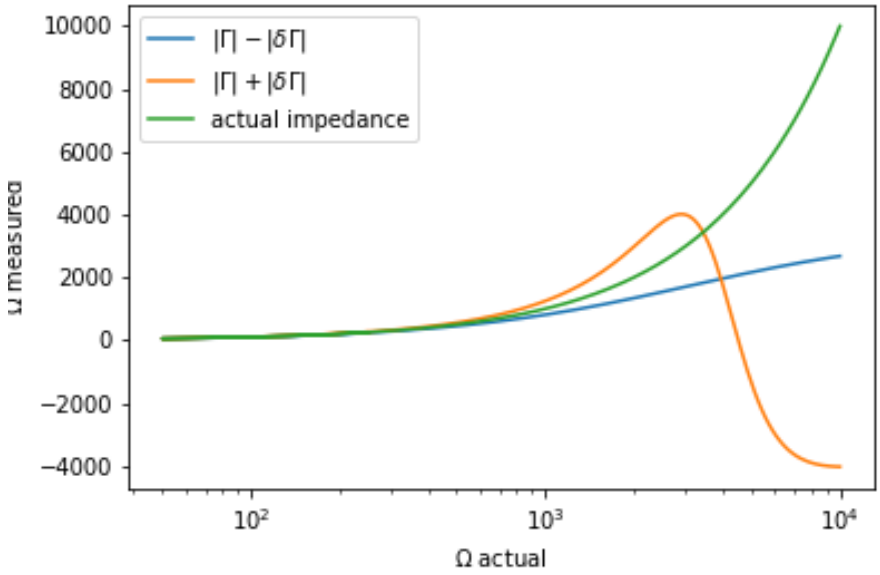

FIG. 15: Measured values of Z with uncertainty in Γ factored in.

with $|\delta\Gamma|$ and $\delta\phi$ the error in magnitude and phase of the reflection coefficient. Substituting 38 into 37 yields

$$\mathbb{R}\mathrm{e}\{Z\} = \quad Z_0 \times \frac{1 - (|\Gamma| + |\delta\Gamma|)^2}{(|\Gamma| + |\delta\Gamma|)^2 \, sin^2(\phi + \delta\phi) + ((|\Gamma| + |\delta\Gamma|) \, cos(\phi + \delta\phi) - 1)^2}$$

$$\mathbb{I}\mathrm{m}\{Z\} = \quad Z_0 \times \frac{2\,(|\Gamma| + |\delta\Gamma|) \, sin\,(\phi + \delta\phi)}{(|\Gamma| + |\delta\Gamma|)^2 \, sin^2(\phi + \delta\phi) + ((|\Gamma| + |\delta\Gamma|) \, cos(\phi + \delta\phi) - 1)^2} \tag{39}$$

These expressions can be used to estimate the error in Z from the error in Γ. Values are

shown in figure 14 of $|\delta\Gamma|$ and $\delta\phi$. Using these values, a real impedance of 500 Ω will read between 548 and 444 Ω, which is an acceptable error. But at 1000 Ω the measurement will be between 1125 and 795 Ω, and 10,000 Ω the reading will be between -1074 and 1904 Ω, which means we're unlikely to reliably read such a large impedance value using this instrument. This is illustrated with figure 15 where we assume real values of impedance on the x-axis and show the values returned by the instrument on the y-axis. The error in phase is negligible for these real impedances and is not included. We can see that at real impedances over a few thousand ohm's the uncertainty in impedance is larger than the impedance itself. This should not be taken to mean that there is no value in measurements of large $\mathbb{R}\text{e}\{Z\}$; rather when we are dealing with such values we should be very cautious in doing any *quantitative* data analysis given the large uncertainty inherent to the measurement.

[1] Steigies CT, Block D, Hirt M, Hipp B, Piel A, Grygoczuk J, *Journal of Physics D* **33** (4): 405 (2000)

[2] Bilen, S.G., Haas, J.M., Gulczinski, F.S. Gallimore, A.D., Letoutchaia, J.N., *AIAA-99-2714*, 35th Joint Propulsion Conference, Los Angeles, CA, June 1999.

[3] Blackwell, D.D., Walker, D.N., Amatucci, W.E., REV SCI INSTRUM vol.76, no.2 : 23503-1-6, (2005)

[4] Blackwell, D.D., Walker, D.N., Messer, S.J., Amatucci, W.E. PHYS PLASMAS vol.12, no.9 : 93510-1-7, (2005)

[5] Blackwell, D.D., Cothran, C.D., et. al., IEEE T PLASMA SCI vol.43, no.8 : 2649-57, (2015)

[6] Jackson, JE, Kane, JA, J GEOPHYS RES 64 (8): 1074-1075 (1959)

[7] Jensen, MD, Baker, KD, J SPACECRAFT ROCKETS 29 (1): 91-95 (1992)

[8] Walker, D.N., Fernsler, R.F., Blackwell, D.D., Amatucci, W.E., Messer, S.J., PHYS PLASMAS vol.13, no.3 : 32108-1-9, (2006)

[9] Walker, D.N., Fernsler, R.F., Blackwell, D.D., Amatucci, W.E., Messer, S.J., PHYS PLASMAS vol.17, 1135039, (2010)

[10] Walker, D.N., Blackwell, D.D., Amatucci, W.E., PHYS PLASMAS vol.22, no.8 : 083505 (2015)

[11] F. B. Llewellyn and L. C. Peterson, Proc. I.R.E. 32, No. 3, 144 (1944)

[12] C.K. Birdsall and W.B. Bridges, *Electron Dynamics of Diode Regions*, chapter 2, Academic Press, New York 1966

[13] Scheiner, B. et. al, Phys. Plasmas 22, 123520 (2015);

[14] Chen, Intro to Plasma Physics and Controlled Fusion

[15] Plasma Sources Sci. and Tech. **18** 2009